BOSE-EINSTEIN CONDENSATES ON MAGNETIC FILM MICROSTRUCTURES

M. SINGH, S. WHITLOCK, R. ANDERSON, S. GHANBARI, B. V. HALL,
M. VOLK, A. AKULSHIN, R. McLEAN, A. SIDOROV AND P. HANNAFORD
ARC Centre of Excellence for Quantum-Atom Optics, and
Centre for Atom Optics and Ultrafast Spectroscopy,
Swinburne University of Technology, Melbourne, Australia 3122
Email: phannaford@swin.edu.au

We report on recent experiments with BECs and ultracold atoms in magnetic microtraps created by magnetic film microstructures on an atom chip. We describe the use of RF spectroscopy plus absorption imaging of ultracold atoms as a sensitive high resolution technique to map the magnetic field topology of the magnetic film. We find that the distribution of condensate atoms between the wells of an asymmetric double-well potential on the magnetic film can provide a highly sensitive technique for determining potential gradients, such as gravitational gradients, using an atom chip. Finally, we report on the use of periodic magnetic film microstructures to generate a magnetic lattice for manipulating BECs and ultracold atoms.

1. Introduction

At the 2001 Laser Spectroscopy conference in Snowbird the Tübingen and Munich groups reported the realization of a Bose Einstein condensate (BEC) in a magnetic microtrap created by current-carrying micro-wires on a substrate [1, 2]. Such 'atom chips' can produce tightly confining magnetic potentials using modest electric currents, thus simplifying and speeding up the production of a BEC. In addition, atom chips allow precise control of the motion and position of the condensate, and they are compact and relatively robust, making them attractive for BEC-based devices and applications. Since Snowbird more than 20 groups around the world have now produced BECs om an atom chip.

The performance of atom chips based on current-carrying conducting wires has, however, certain limitations. Current instabilities and current noise can limit the lifetime and coherence properties of a condensate, and high current densities can lead to excessive heating and breakdown of the conductors [3]. In addition, small imperfections in the wires can lead to tiny spatial deviations in the current flow which can fragment the atom cloud [4], while thermal fluctuations associated with Johnson noise in the conducting wires can lead to spin flips and a loss of atoms close to the surface of the chip [5, 6].

At the last Laser Spectroscopy conference, in Aviemore, we reported the observation of a BEC on a *permanent* magnetic film atom chip [7, 8] based on perpendicularly magnetised TbGdFeCo magneto-optical films previously developed for our atom optics experiments [9-11]. Magnetic film microstructures can produce highly stable, tightly confining magnetic potentials without ohmic heating, and they can produce very fine-structured magnetic potentials, with periodicities down to about 1 μm [11], and complex magnetic potentials such as ring-shaped structures. Although the potentials from magnetic film microstructures are necessarily static, they can be combined with magnetic potentials from current-carrying conductors when time-dependent magnetic fields are required, e.g., when loading the atom chip. BECs on permanent-magnet atom chips have also recently been produced using videotape [12], a CoCrPt hard disk [13] and FePt thin films [14].

In this paper we report on recent experiments with BECs and ultracold atoms on perpendicularly magnetised magnetic film microstructures on an atom chip. We describe a sensitive high resolution technique based on RF spectroscopy plus absorption imaging of ultracold atoms to map the magnetic topology of the magnetic film. [15]. We find that the distribution of condensate atoms between the wells of an asymmetric double-well potential on the magnetic film can provide a highly sensitive technique for determining potential gradients, such as gravitational gradients, using an atom chip [16]. Finally, we report on the use of *periodic* magnetic film microstructures to generate a magnetic lattice for manipulating BECs and ultracold atoms [17-19]

2. The Magnetic Film Atom Chip

Our atom chip consists of a perpendicularly magnetised 1 μm-thick TbGdFeCo magneto-optical film deposited on a 300 μm-thick glass substrate mounted on a silver foil 'circuit', which provides time-dependent magnetic fields for initial trapping and loading of ultracold atoms in the magnetic film trap. The silver circuit has U- and Z-shaped wires for a surface magneto-optical trap (MOT) and a Ioffe-Pritchard magnetic trap. The magnetic film microtrap is produced by the field above an edge of the film plus a bias field B_{bias} to provide radial confinement and two end-wires to provide weak axial confinement [8] (Fig. 1).

The magneto-optical films are prepared in-house by magnetron sputtering at substrate temperatures of 100–200^{o}C [11]. We typically use films comprising six 150 nm layers of $Tb_{10}Gd_6Fe_{80}Co_4$ separated by 100 nm layers of Cr. The films have high perpendicular anisotropy with excellent magnetic homogeneity, high remanent magnetization (~ 3 kG), high coercivity (~ 2 kOe) and a

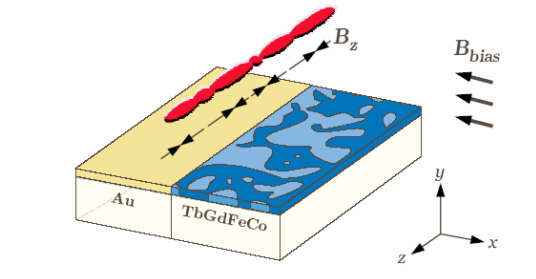

Figure 1. Schematic of the magnetic film atom chip. Long range inhomogeneity in the magnetic film leads to fragmentation of the trapped atom cloud when close to the surface. After [15].

nominally high Curie temperature (~ 300°C). The magneto-optical films are coated with a reflecting gold film for use in a mirror MOT. The atom chip is mounted in the vacuum chamber with the magnetic film facing down.

Initially, about 2 x 10^8 ^{87}Rb atoms are collected in the mirror MOT located 5 mm below the surface, optically pumped into the $|F=2, m_F=+2\rangle$ trapping state and subsequently transferred to the Z-wire microtrap. After a preliminary RF evaporative cooling stage, the atoms are transferred to the magnetic film microtrap by adiabatically reducing the current in the Z-wire to zero. Forced RF evaporative cooling of the atom cloud in the magnetic film microtrap leads to a BEC with about 10^5 atoms [7, 8]. Temperature measurements on a dilute cloud of ultracold atoms indicate a remarkably low heating rate of 3 nK s^{-1} in the magnetic film trap, compared with 270 nK s^{-1} in the Z-wire trap, and a trap lifetime of about 5 s, which is limited by time-varying stray magnetic fields.

3. Spatially Resolved RF Spectroscopy to Probe Magnetic Field Topology

The small kinetic energies and small spatial extent of the cloud of ultracold atoms can provide a sensitive high resolution (~ 5 μm) probe of corrugations in the magnetic potential [20]. Here, we employ precision RF spectroscopy plus high resolution imaging of trapped ultracold atoms to probe the magnetic field topology along the edge of the magnetic film [15].

After allowing the atom cloud to expand along the 5 mm edge of the magnetic film by reducing the current in the end-wires, a ramped RF field is applied perpendicular to the trap axis to resonantly out-couple atoms to untrapped magnetic states at positions where the RF frequency matches the Zeeman splitting of the atoms. At the end of the ramp the resonant frequency approaches a final cut-off frequency ν_f corresponding to the bottom of the trap, and the atom distribution is described by a truncated Boltzmann distribution which is characterised by a spatially dependent truncation parameter [15].

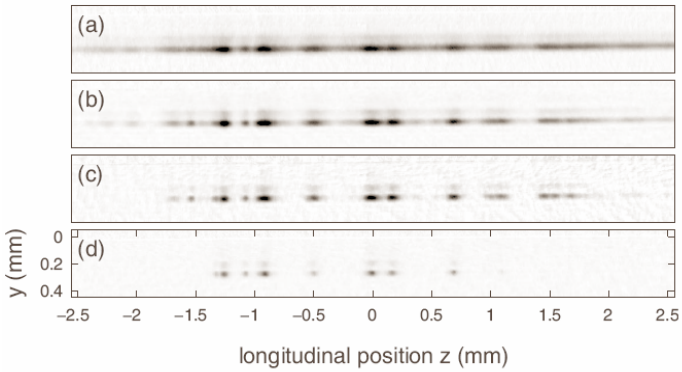

Figure 2. Absorption images for a ^{87}Rb cold atom cloud in the magnetic microtrap located 67 μm below the edge of the magnetic film, for a RF cut-off frequency ν_f of (a) 1238 kHz, (b) 890 kHz, (c) 766 kHz and (d) 695 kHz. Trap parameters: $B_{\rm bias}$ = 5.7 G, field offset B_0 = 0.82 G, $\omega_r = 2\pi \times 1070$ Hz. Initial cloud temperature $T = 10$ μK. After [15].

$$\beta\,(z, \nu_f) = [m_F h \nu_f - m_F g_F \mu_B |\, B_z(z) + B_0 |\,]/k_B T,$$

where B_0 is an offset field and T is a fit parameter that characterises the non-equilibrium distribution during truncation.

Figure 2 shows absorption images for a cold atom cloud in the magnetic microtrap located 67 μm below the magnetic film edge for four values of the RF cut-off frequency ν_f. For $\nu_f < 1.3$ MHz significant fragmentation of the atom cloud is observed, and for $\nu_f < 0.9$ MHz well separated regions appear corresponding to atoms in the lowest potential wells. Using an iterative procedure we extract values of $|B_{z,y}(z)|$ and obtain the reconstructed magnetic field profiles shown in Fig. 3 for a number of trap heights. We find that the amplitude of the observed magnetic corrugations falls off with distance y as $y^{-1.85 \pm 0.3}$. The characteristic period of the corrugations is about 390 μm for $y > 100$ μm with additional higher frequency components appearing as the atom cloud is brought closer to the film.

The amplitude of the corrugated potential is about three orders of magnitude larger than that estimated from the roughness (~ 50 nm) of the polished film edge, but is consistent with the y^{-2} behaviour predicted for long range inhomogeneities in the magnetisation of the film [15]. Investigating this further, measurements taken with the atom cloud positioned below the magnetic film at $x = 100$ μm from the edge show significant fragmentation while those recorded below the non magnetic film at $x = -100$ μm from the edge show almost no corrugation, thus confirming that the fragmentation results from spatial variations of the magnetisation in the body of the magnetic film rather than from fluctuations along the edge of the film.

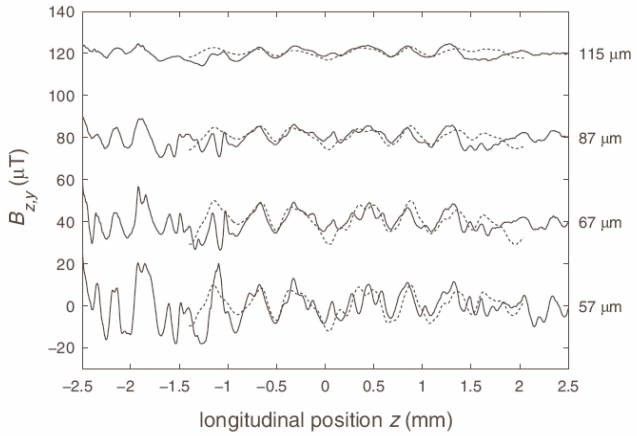

Figure 3. Magnetic field profiles $B_z(z)$ measured using spatially resolved RF spectroscopy (solid lines) for various distances y below the edge of the magnetic film. The dotted lines correspond to measurements of the magnetic film edge using a scanning magneto-resistance probe, which measures the B_y component of the corrugated magnetic field. The relative longitudinal offset has been adjusted for optimal agreement. After [15].

After removing the magnetic film atom chip from the vacuum chamber, the magnetic corrugation was further characterised using a home-built magneto-resistance microscope, which allows measurements over a wide range of distances with a spatial resolution of about 50 μm. The magneto-resistance measurements, indicated by the dotted lines in Fig. 3, show a remarkable correlation with the RF spectroscopy cold atom data, thus verifying the validity of the RF spectroscopy cold atom technique.

The observed magnetic inhomogeneity in the magnetic films is attributed to deterioration during vacuum bake out of the magnetic film atom chip (140^{o}C for 4 days). Assuming the inhomogeneity originates from reversal of magnetic domains, we conclude that the mean magnetisation of the film is about 90% of the saturation value. After remagnetising the film the level of inhomogeneity was reduced by about a factor of 10.

4. Dynamic Splitting of a BEC in an Asymmetric Double Well

In the reconstructed magnetic field profiles in Fig. 3, we identify a double-well potential in the region near $z = 0$ when the magnetic trap is brought close to the surface of the film by increasing B_{bias} in the x direction [16]. The double well originates from higher spatial frequency components of the magnetisation inhomogeneity at distances close to the magnetic film.

Figure 4 (left) shows a series of high resolution absorption images as a BEC is slowly brought (in 0.5 s) from about 170 μm below the film, where the

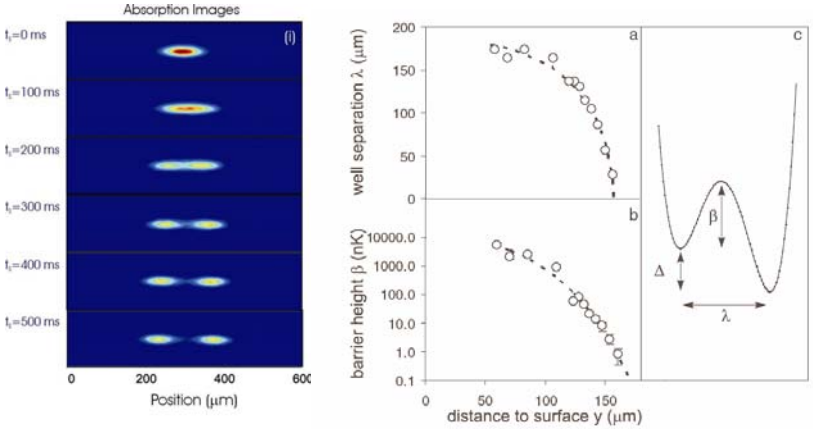

Figure 4. Left: dynamic splitting of a BEC in a double-well potential. High resolution absorption images are shown as the BEC is slowly moved from about 170 μm below the film to about 57 μm below the film. Right: characterisation of the double-well potential as a function of trap-surface separation is performed using two-component clouds. The well separation λ, barrier height β and trap asymmetry Δ are shown schematically in (c). After [16].

potential behaves as a single well, to 57 μm below the film, where it behaves as a double well. Under these conditions the BEC dynamically splits into two, with about equal numbers of atoms in each well.

The double well is characterised by taking absorption images for various trap heights y and determining the well separation λ and barrier height β as a function of y (Fig. 4, right) [16]. The trap frequencies of the two wells, obtained from dipolar oscillations, are identical within a few percent. The asymmetry Δ in the double well can result in a marked difference in the number of atoms in the two wells when the barrier height β < the chemical potential μ.

Slight tilts of the atom chip with respect to gravity, e.g., from tiny movements of the optical table, were found to have a marked effect on the distribution of the condensate between the two wells. The gravitational gradient is cancelled by applying a small magnetic field gradient provided by a current imbalance $\pm \delta I$ between the two end-wires on the chip. The trap asymmetry Δ can be calibrated *in situ* against δI by adiabatically splitting a condensate in a *symmetric* double well with barrier height β > μ and using spatially resolved RF spectroscopy, as described in Sect. 3. A condensate with a relatively small number of atoms is initially prepared in a single well at $y = 170$ μm below the film and then B_{bias} is slowly increased to produce a tailored double well at $y = 155$ μm, where the well separation λ ≈ 70 μm and the barrier height β ≈ ¼ μ. The splitting time t_S is chosen to be larger than Δ^{-1} to ensure the condensate remains in the ground state of the potential well.

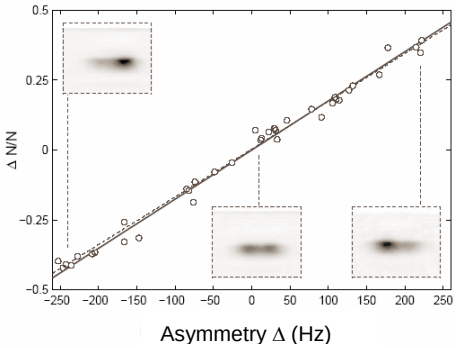

Figure 5. Fractional number difference versus asymmetry Δ of a double-well potential. The asymmetry is varied by changing the end-wire current imbalance δ*I*. The experimental points and line of best fit (dashed line) compare well with the simple analytic result (solid line). After [21].

Absorption images of the condensate are then recorded as δ*I* is ramped over ± 117 mA, and the fractional atom number difference $(N_R + N_L)/(N_R - N_L) = \Delta N/N$ is recorded against δ*I*, and hence Δ. From the distribution of the data (Fig. 5) we estimate a single-shot sensitivity $\Delta_{SNR} \approx 16$ Hz, which is limited by the shot-to-shot variation in the number of atoms in the condensate. From this result we infer a single-shot sensitivity to gravity gradients of $\delta g/g \approx 2 \times 10^{-4}$.

Using a simple model in which the double-well potential is represented by two uncoupled 3D harmonic oscillators we obtain [16]

$$\Delta N/N \approx 1.65\ (4\pi)(a_0/15aN)^{2/5}\ \Delta/\varpi,$$

where a is the scattering length, a_0 is the ground state harmonic oscillator length, and ϖ is the geometric mean trap frequency. Inserting experimental parameters into this expression yields a straight line in good agreement with the experimental data (Fig. 5). The sensitivity could be further enhanced by decreasing the trap frequency ϖ, thereby lowering the chemical potential μ, or by using multiple double-well potentials on a single chip. For 100 double wells and reasonable values for the parameters we estimate a possible single-shot sensitivity of $\Delta_{SNR} \approx 0.04$ Hz, or $\delta g/g \approx 5 \times 10^{-7}$.

5. Periodic Magnetic Lattices

Optical lattices produced by the interference of intersecting laser beams are widely used to manipulate BECs and clouds of ultracold atoms, e.g., in quantum tunnelling experiments. Here, we report on the use of periodic magnetic lattices based on permanent magnetic films as an alternative to optical lattices [17-19].

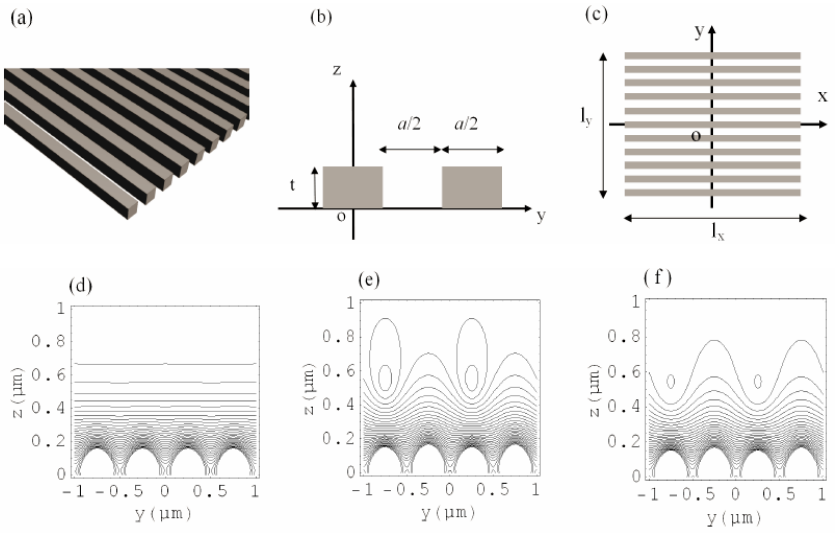

Figure 6. (a)–(c) 1D periodic array of parallel magnets with perpendicular magnetisation. (d)–(f) Calculated contour plots of the magnetic field in the central region in the *y*0*z* plane with (d) no bias fields, (e) bias field $B_{1y} = -15$ G, and (f) bias fields $B_{1x} = -20$ G, $B_{1y} = -15$ G. 1001 magnets, $a = 1$ μm, $t = 0.05$ μm, $l_x = 1000.5$ μm, and $4\pi M_z = 3.8$ kG. 7 G contour spacing. After [17].

Magnetic lattices based on magnetic films have a number of distinctive characteristics: (i) They are highly stable with low technical noise; (ii) There is no spontaneous emission; (iii) The atoms need to be prepared in low magnetic field-seeking states, allowing RF evaporative cooling *in situ* and the use of spatially resolved RF spectroscopy; (iv) They can have large and controllable barrier heights and large trap curvature leading to high trap frequencies; (v) They can be constructed with a wide range of periods, down to about 1 μm, and they can have complex potential shapes; (vi) They are necessarily static, precluding use in time-dependent lattice experiments; and (vii) 2D and 1D magnetic lattices, but not 3D, can be constructed. Thus magnetic lattices can be considered as complementary to optical lattices, in much the same way as magnetic traps are complementary to optical dipole traps.

We first consider a simple 1D magnetic lattice produced by a single periodic array of parallel magnets of thickness t with perpendicular magnetisation, period a, and bias fields B_{1x} and B_{1y} parallel and perpendicular to the grooves, respectively (Fig. 6) [17]. For $B_{1x} = B_{1y} = 0$ (Fig. 6(d)), the magnetic field falls off exponentially with distance z above the surface, representing the case of a magnetic mirror [9, 10]. For $B_{1x} = 0$, $B_{1y} = -15$ G (Fig. 6(e)), the magnetic field develops 2D magnetic traps with zero potential minima; this configuration can give rise to spin flips and is not suitable as a

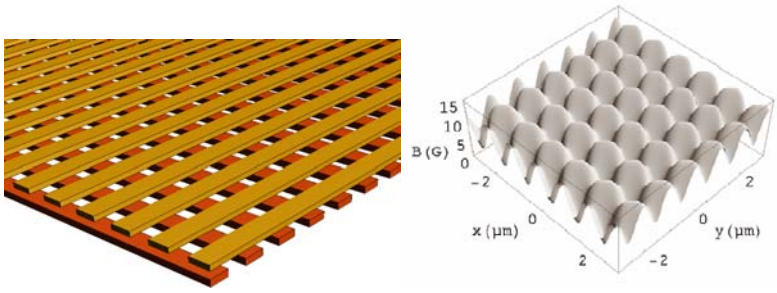

Figure 7. (a) 2D periodic array consisting of two crossed layers of parallel magnets with perpendicular magnetisation. (b) 3D plot of the magnetic field. 1001 magnets, $a = 1$ μm, $t_1 = 0.322$ μm, $t_2 = 0.083$ μm, $l_x = l_y = 1000.5$ μm, $4\pi M_z = 3.8$ kG, $B_{1x} = -4.08$ G, $B_{1y} = -6.05$ G, $B_{1z} = -0.69$ G. $B_{\min} = 2.7$ G, $z_{\min} = 1.22$ μm, $\Delta U^x = \Delta U^y = 485$ μK, $\Delta U^z = 307$ μK, $\omega_x = \omega_x = 2\pi \times 232$ kHz, $\omega_z = 2\pi \times 329$ kHz. After [17].

lattice. For $B_{1x} = -20$ G, $B_{1y} = -15$ G (Fig. 6(f)), the magnetic field has 2D magnetic traps with non zero potential minima.

For an infinite 1D magnetic lattice, the potential minimum, trap height, and barrier heights are given by [17]

$$B_{\min} = |B_{1x}|; \; z_{\min} = (a/2\pi) \ln [B_{0y} / |B_{1y}|]$$

$$\Delta B^{\,y} = (B_{1x}^{\,2} + 4\, B_{1y}^{\,2})^{1/2} - |B_{1x}|; \quad \Delta B^{\,z} = (B_{1x}^{\,2} + B_{1y}^{\,2})^{1/2} - |B_{1x}|$$

where $B_{0y} = B_0 (1 - e^{-kt}) e^{kt}$ and $k = 2\pi/a$. The potential minimum, trap height and barrier heights can be controlled by means of the bias fields B_{1x} and B_{1y}.

We now consider a 2D magnetic lattice produced by two crossed periodic arrays of parallel magnets, thicknesses t_1 and t_2, separated by distance s ($< a/2\pi$), and with bias fields B_{1x}, B_{1y} (Fig. 7(a)). Figure 7 (b) shows the calculated magnetic field for the parameters given in the caption. For an infinite *symmetrical* 2D magnetic lattice, the trap minimum, trap height, and barrier heights are given by [17]

$$B_{\min} = c_1 |B_{1x}|; \; z_{\min} = (a/2\pi) \ln (c_2 B_{0x} / |B_{1x}|)$$

$$\Delta B^{\,x} = \Delta B^{\,y} = c_4 |B_{1x}|; \quad \Delta B^{\,z} = c_5 |B_{1x}|$$

with the constraint $B_{1y} = c_0 B_{1x}$ for a symmetrical lattice. The c_i's are dimensionless constants that involve geometrical constants a, s, t_1 and t_2 of the magnetic arrays and $B_{0x} = B_0 (1 - e^{-kt_2}) e^{k(s+t_1+t_2)}$. The potential minimum, trap position and barrier heights can be controlled by varying B_{1x} and B_{1y}. Other configurations of 2D magnetic lattices have also been proposed [17, 19].

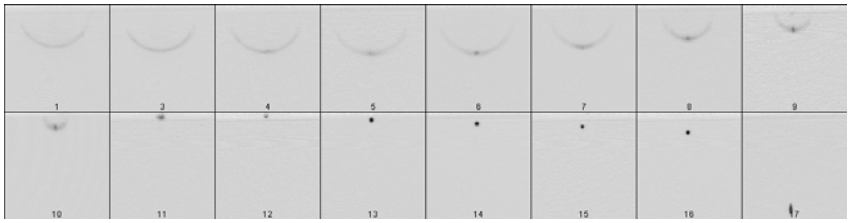

Figure 8. Absorption images, after 8 ms time of flight, of a ^{87}Rb condensate after it has been brought to various distances below the 10 μm-period magnetic microstructure, ranging from $z \sim 6$ μm (first image) to $z \sim 150$ μm (final image). $B_y = 0$ (perpendicular to grooves).

6. Realisation of a Permanent-Magnet Lattice for Ultracold Atoms

We have constructed a 1D magnetic lattice with period $a = 10$ μm and dimensions 10 mm × 10 mm using a six-layer structure of perpendicularly magnetised TbGdFeCo magneto-optical films deposited on a grooved silicon wafer. The magnetic microstructure is coated with a reflecting gold film for use in the mirror MOT. The magnetic microstructure is mounted on an atom chip, similar to that described in Sect. 2, but with a 30 mm long Z-wire, in addition to the 5 mm long Z-wire, perpendicular to the grooves for effective loading of ultracold atoms into the magnetic lattice. To ensure minimal demagnetisation during vacuum bakeout care was taken not exceed a temperature of 100°C.

First, a BEC with $\sim 2 \times 10^5$ ^{87}Rb atoms is prepared in the 5 mm Z-wire trap 250 μm below the chip surface where the magnetic microstructure has a negligible effect. The current in the Z-wire is then slowly ramped down to bring the condensate closer to the surface so that it interacts with the magnetic microstructure for less than 5 ms before being released. In this initial experiment the bias field perpendicular to the grooves was switched off, so the microstructure is not yet a trapping magnetic lattice. Absorption images are taken after a time of flight (TOF) of 8 ms. As the condensate is brought closer (from ~ 150 μm to ~ 6 μm) to the magnetic microstructure, the TOF images change from a tiny cloud to sharply defined crescent-shaped structures, indicating that the condensate has interacted with the magnetic microstructure. The crescent-shaped structures are attributed to reflection of the atoms from a periodic corrugation in the magnetic potential caused largely by a magnetic field produced by residual current in the Z-wire. When the temperature of the atom cloud is raised above the BEC transition the crescent-shaped structures broaden markedly due to the larger trap volume. Bias fields of $B_{1x} = -15$ G, $B_{1y} = -30$ G are then turned on to create a magnetic lattice of 2D traps with a barrier height of about 1.2 mK. Absorption images taken after loading about

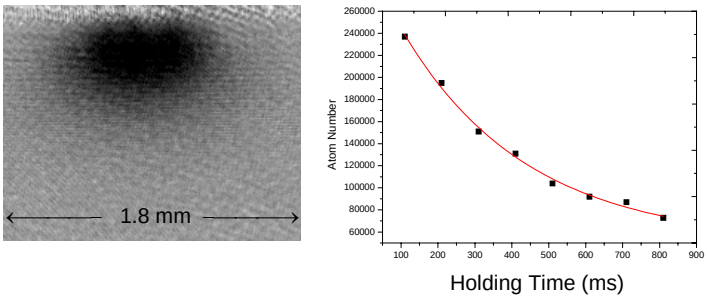

Figure 9. Left: Absorption image, after 14 ms time of flight, of a thermal cloud of ~ 5×10^5 ^{87}Rb atoms at 15 μK trapped in a 10 μm-period 1D magnetic lattice at 6 – 8 μm from the surface of the atom chip. $B_x = -15$ G, $B_y = -30$ G. The image is taken in a direction parallel to the grooves. Right: Decay of the thermal cloud after release from the magnetic lattice. The lifetime is 0.34 s.

5×10^5 ^{87}Rb atoms in a 15 μK thermal cloud from the 5 mm Z-wire trap into the 10 mm × 10 mm magnetic lattice and after14 ms TOF indicate that atoms are
trapped in about 100 of the 1000 lattice sites at 6 – 8 μm from the surface (Fig. 9, left). By releasing the atoms from the magnetic lattice, the lifetime of the atoms trapped in the magnetic lattice is found to be 0.34 s (Fig. 9, right). With our current pixel image resolution of 9 μm it was not possible to resolve atoms in individual lattice sites of the 10 μm-period magnetic lattice. We also note that at this resolution there is little evidence of fragmentation even though the atoms are trapped very close (6 – 8 μm) to the magnetic microstructure.

In future it should be possible to populate a large fraction of the 1000 lattice sites, by loading from the 30 mm long Z-wire trap, and to resolve atoms in the individual lattice sites using spatially resolved RF spectroscopy. We also plan to implement RF evaporative cooling on the trapped atom clouds to create condensates on individual sites of the magnetic lattice and to study the diffraction of the condensate atoms when released from the magnetic lattice. We also plan to implement a 2D magnetic lattice on an atom chip and to construct magnetic lattices with smaller periods (1–5 μm) in order to study quantum tunnelling in 1D and 2D magnetic lattices. One of the major challenges will be to fabricate periodic magnetic microstructures having sufficiently smooth magnetic potentials very close to the surface to produce high-quality small-period magnetic lattices that preserve quantum coherence.

During the preparation of this manuscript a preprint appeared in which ultracold rubidium atoms were trapped in > 30 lattice sites of a 2D FePt magnetic lattice with period 20 μm [22].

7. Summary

We have implemented perpendicularly magnetised magnetic film micro-structures to trap and manipulate BECs and ultracold atoms on an atom chip. We have developed a sensitive high resolution technique, based on RF spectroscopy plus absorption imaging of ultracold atoms, to map the magnetic field topology of the magnetic film. We have used a double-well potential close to the magnetic film to dynamically split a BEC. We find that the distribution of condensate atoms between the two wells can provide a highly sensitive technique for determining potential gradients, such as gravitational gradients, on an atom chip. Finally, we have loaded and trapped small clouds of ultracold atoms in a 1D permanent-magnet lattice on an atom chip.

Acknowledgments

This project is supported by the ARC Centre of Excellence for Quantum-Atom Optics and a Swinburne University Strategic Initiative grant.

References

1. H. Ott *et al*., *Phys. Rev. Lett.* **87**, 230401 (2001).
2. W. Hänsel *et al*., *Nature* **413**, 498 (2001).
3. D. C. Lau *et al*., *Eur. Phys. J.* D **5**, 193 (1999).
4. D. W. Wang *et al*., *Phys. Rev. Lett.* **92**, 076802 (2004).
5. M. P. A. Jones *et al*., *Phys.Rev. Lett.* **91**, 080401 (2003).
6. J. Estève *et al*., *Phys. Rev.* A **70**, 043629 (2004).
7. B. V. Hall *et al*., *Laser Spectroscopy XVII*, (World Scientific, 2005), 275.
8. B. V. Hall *et al*., *J. Phys. B: At. Mol. Opt. Phys.* **39**, 27 (2006).
9. A. Sidorov *et al*., *Compt. Rend.* **2**, Series IV, 565 (2001).
10. A. Sidorov *et al*., *Acta Phys. Pol.* B **33**, 2137 (2002).
11. J. Y. Wang *et al*., *J. Phys. D: Appl. Phys.* **38**, 4015 (2005).
12. C. D. J. Sinclair *et al., Phys. Rev.* A **72**, 031603(R) (2005).
13. M. Boyd *et al.*, preprint cond-mat/0608370 (2006).
14. T. Fernholz *et al*., preprint cond-mat/07052569 (2007).
15. S. Whitlock *et al*., *Phys. Rev.* A **75**, 043602 (2007).
16. B. V. Hall *et al*., *Phys. Rev. Lett.* **98**, 030402 (2007).
17. S. Ghanbari *et al*., *J. Phys. B: At. Mol. Opt. Phys.* **39**, 847 (2006).
18. R. Gerritsma and R. J. C. Spreeuw, *Phys. Rev.* A **74**, 043405 (2006).
19. S. Ghanbari *et al*., *J. Phys. B: At. Mol. Opt. Phys.* **40**, 1283 (2007).
20. S. Wildermuth *et al*., *Nature* **435**, 440 (2005).
21. S. Whitlock, PhD Thesis, Swinburne University of Technology, 2007.
22. R. Gerritsma *et al*., preprint physics/07061170 (2007).